


 Cite this: *RSC Adv.*, 2024, **14**, 37240

Eco-friendly impact of a novel green *Melilotus officinalis* extract as a sustainable inhibitor to reduce acid corrosion of copper

 Abd El-Aziz S. Fouda, ^{*a} Salah M. Rashwan, ^b Medhat M. Kamel, ^b Mohamed Atef ^b and Ahmed El-Hossiany ^{ac}

In this study, we deployed green *Melilotus officinalis* extract (MOE) as a corrosion inhibitor for copper. The anticorrosion properties of MOE for Cu in 1 M HNO₃ were investigated by various experimental and numerical techniques, including potentiodynamic polarization (PDP), electrochemical impedance spectroscopy (EIS), and a weight loss (WL) method at different temperatures. Additionally, scanning electron microscopy (SEM) coupled with energy-dispersive X-ray analysis (EDX) and atomic force microscopy (AFM) were utilized to examine the surface morphology of Cu with and without the extract. By contrasting the inhibition effectiveness with and without the extract, the inhibition efficiency (% IE) was observed. The WL method revealed that 300 ppm of the extract had an IE of 93.8% for Cu immersed in one molar HNO₃ solution. The MOE was classified as a mixed type according to the PDP study since it delayed both cathodic and anodic processes, with a cathodic predominance. At 25–45 °C, MOE's free adsorption energies were 23.1–21.5 kJ mol⁻¹, showing that mixed-type adsorption occurred on the Cu surface. Additionally, the Langmuir adsorption isotherm and the adsorption data from the WL tests of MOE showed a good match. The extract could adsorb spontaneously onto the metal surface, according to the thermodynamic conditions. Analysis of the corrosion product using different techniques revealed that a protective layer had formed on the metal's surface. Hence, MOE had a good corrosive inhibitive effect on Cu in HNO₃ solution. It turned out that all the methods used gave consistent results.

Received 25th July 2024

Accepted 1st November 2024

DOI: 10.1039/d4ra05391e

rsc.li/rsc-advances

1. Introduction

Copper is one of the most commonly utilized metals for both industrial and residential applications, due to its many advantages, including its low cost, strong mechanical workability, and excellent electrical conductivity. However, copper can readily corrode due to a variety of environmental factors. The most common corrosive solution for copper is nitric acid.¹ Corrosion is an electrochemical process involving anodic and cathodic reactions on the surface of metals.² Any alteration in the physical components of metals, due to physicochemical contact with their environment, that results in deterioration of the metal's character is called corrosion.³ Corrosion is an expensive, as well as harmful issue. Every year, billions of dollars are spent on repairing corroded buildings, equipment, and parts as early failure could lead to the loss of human life and security damage. By adding chemical compounds to a corroding material, the surface metal corrosion can be controlled and minimized. The

most effective method for dealing with corrosion of metals is using inhibitors. A corrosion inhibitor is a substance that, when added in small amounts to the corrosive solution, lowers the corrosion rate of the metal. In recent studies, not only have new inhibitors with high inhibition efficiency been developed, but also with other characteristics, such as low-cost, low-toxicity, and readiness for production processes.⁴ The use of inhibitors is the most practical method for defending against the successive dissolution of a metal by corrosion. The use of O-, S-, and N-containing organic compounds to minimize metal corrosion has been studied.⁵ The presence of heteroatoms in the inhibitor's chemical structure plays a significant role in the action of corrosion inhibition. Other factors have a significant influence on the efficiency of inhibition too, such as the molecular weight, aromatic rings, and inhibited metal load.⁶ Several papers were found in the literature related to the use of plant extracts as corrosion inhibitors for metals. For instance, the use of a pectin eco-friendly natural polymer as a corrosion inhibitor on mild steel in hydrochloric media demonstrated maximum inhibition efficiencies of 91.5% and 93.9% obtained using 1 g L⁻¹ of both acid- and enzyme-extracted pectin, respectively.⁷ The extracts from *Aloe vera* leaves were studied in 1 M H₂SO₄ solution. The results indicated that the plant extract acts as a mixed-type

^aDepartment of Chemistry, Faculty of Science, Mansoura University, Mansoura-35516, Egypt. E-mail: asfouda@mans.edu.eg

^bDepartment of Chemistry, Faculty of Science, Suez Canal University, Egypt

^cDelta Fertilizers Company in T alkha, Egypt



inhibitor for mild steel with an IE% of 98% at a 30% v/v concentration.⁸ An extract from *Ricinus* was studied to reduce the mild steel corrosion in aqueous solution. The extract showed an IE% of 84% at a 300 ppm concentration.⁹ The effect of *Ficus carica* leaf extract on steel anticorrosion in petroleum solution was investigated,¹⁰ and the results indicated that the extract had an IE% of 70–80% at 298 K. The influence of *Citrus aurantium* leaves extract on mild steel corrosion in 1 M H₂SO₄ was studied by K. H. Hassan *et al.*¹¹ Using the WL method, a maximum inhibition efficiency of 89% was obtained at 313 K with 10 mL L⁻¹ of the leaves. Mango (*Mangifera indica*) extract was used as an inhibitor of the corrosion phenomenon affecting mild steel in 1 M H₂SO₄ in various methods.¹² In this situation, the measurements were carried out at temperatures of 303–333 K. The results showed that the best inhibition efficiency of 74% was obtained at an inhibitor concentration of 0.97 g L⁻¹ and temperature of 303 K. R. T. Loto¹³ investigated the inhibitory action of a combined admixture of *Rosmarinus officinalis* and zinc oxide on low carbon steel in 1 M HCl and H₂SO₄ solutions. Maximum inhibition efficiencies of 93.26% in HCl and 87.7% in H₂SO₄ acid solutions were observed. F. Bouhllal *et al.*¹⁴ analyzed coffee grounds extract as an inhibitor of the corrosion of C38 steel in 1 M hydrochloric acid medium. A high inhibition efficiency of 97.4% was achieved with 2 g L⁻¹. H. Lahbib *et al.*¹⁵ used various methods to examine the inhibiting effect of dwarf palm and *Cynara cardunculus* leaves extract for St37 steel in 15% H₂SO₄ solution. High inhibition efficiencies of 76.13% and 69.35% were obtained with 30 ppm of dwarf palm and *Cynara cardunculus* leaves extracts, respectively. On the other hand, several authors (Table 1) have used plants extracts as inhibitors for copper to lessen metal corrosion in a variety of common industrial solutions.^{16–30}

Nevertheless, there are no further reports of MOE being used as an inhibitor. Therefore, the goal of this work was to estimate the inhibitory action of MOE against the corrosion of Cu in nitric acid solution using a WL method, and electrochemical techniques (potentiodynamic polarization (PDP) and electrochemical

impedance spectroscopy (EIS)). These measurements were supplemented by SEM, EDX, AFM, and FTIR.

2. Experimental section

First, 1 M nitric acid (HNO₃) was prepared in the laboratory by diluting an appropriate volume of analytical grade 69% HNO₃ with bi-distilled water. For the WL tests, the composition of the Cu samples was: Sn (0.001), Fe (0.01), Bi (0.005), Pb (0.002), and Cu (rest) as a percentage by weight. Prior to every experiment, the Cu samples were washed with acetone and double-distilled water, dried, and ground using SiC sheets graded 600–1200. A Cu plate with the dimensions of 2 cm × 2 cm × 0.1 cm was used for the samples. For the electrochemical tests, the Cu sheet was welded with Cu wire for electrical connection and inserted into a Teflon tube and fixed with an adhesive. The area exposed to the solution was 1 cm². The samples underwent treatment as before.

2.1 *Melilotus officinalis* (MOE) procedure

The fresh MOE parts were first prepared by dehydration, followed by milling to a powder. Then, 500 g of the powder was immersed in methanol, and boiled at 100 °C, and then left to stand at room temperature for about 72 h. After that, the MOE was filtrated and placed in the air to dry. In order to attain a 1000 ppm stock solution of the extract, 1 g of the dried MOE was dissolved in 1 L double-distilled water. In addition to the control, different dosages (from 50 to 300 ppm) were prepared from the stock solution and their anticorrosion effects were tested. The main components of MOE, comprising two new *p*-hydroxybenzoic acid glycosides, namely *p*-hydroxybenzoic acid-4-*O*- α -D-manopyranosyl-(1 → 3)- α -L-rhamnopyranoside and 4-*O*- α -L-rhamnopyranosyl-(1 → 6)- α -D-manopyranosyl-(1 → 3)- α -L-rhamnopyranoside, and seven known compounds as acid components, flavonoids, a coumarin, and an alkaloid, were isolated from the 70% ethanol aqueous extract of the aerial parts of *Melilotus officinalis*.³¹

Table 1 Lists of plant extracts used as Cu corrosion inhibitors

Inhibitor (extract)	Medium	% IE	Ref.
<i>Moringa oleifera</i>	1 M H ₃ PO ₄ + HNO ₃	73.5 at 300 ppm	16
<i>Idesia polycarpa</i> maxim fruits	0.5 M H ₂ SO ₄	75–86	17
Cannabis plant	0.5 M H ₂ SO ₄	91 at 25 ppm	18
Cinnamon essential oil	3 wt% NaCl	89.0	18
<i>Ephedra sarcocarpa</i> (ES)	2 M HCl	95 at 0.5 g L ⁻¹	19
Acid extract of <i>Azadirachta indica</i> seed	1–3 N HNO ₃	95 at 1% extract	20
Mangrove tannin	0.5 M HCl	82 at 3 g L ⁻¹	21
Caffeine isolated from black tea	0.5 NaCl	92	22
<i>Calligonum comosum</i>	2 M HCl	80.06% in 0.8 g L ⁻¹	23
Alcoholic extract of <i>Mimusops elengi</i> leaves	Natural sea water	86.84	24
<i>Alhagi maurorum</i> plant	0.5 M H ₂ SO ₄	90	25
Olive leaf extract	0.5 M NaCl	90	26
<i>Capparis spinosa</i> L	Strong acid media	82.7 at 440 ppm	27
<i>Ziziphus lotus</i>	Sea water	93 at 5 g L ⁻¹	28
Berry leaves	2 M HNO ₃	90.1 at 300 ppm	29
Olive leaf	0.5 M NaCl	95	30
<i>Melilotus officinalis</i> (MOE)	1 M HNO ₃	93.8 at 300 ppm	Our results

2.2 WL measurements

The American Society for Testing and Materials (ASTM) provides standardized procedures for conducting various types of corrosion tests, ensuring consistency and reliability in results.³² After being ground, cleaned, dried, and weighed, the Cu samples were suspended in 100 mL of 1 M HNO₃ solution with and without different MOE dosages (50–350 ppm) for 60–360 min at different temperatures (25–45 °C) for investigation. After the designated exposure period, the Cu samples were removed, cleaned carefully with double-distilled water to eliminate the corrosion products, dried with filter papers, and weighed precisely according to the standard method. The loss in weight was estimated by the difference in weight of Cu samples before and after the exposure. Every measurement was performed in triplicate³³ for assessing the reproducibility. The assessed WL can be used to determine the Cu surface area that is covered (θ) and the effectiveness of inhibition (% IE) by the following equation:

$$\% \text{ IE} = \theta \times 100 = \left(1 - \frac{\Delta W_{\text{inh}}}{\Delta W_{\text{free}}} \right) \times 100 \quad (1)$$

where the WL (mg) with and without MOE are represented by ΔW_{inh} and ΔW_{free} , respectively. Following are the formulas for calculating the rate of the corrosion process (k_{corr}):

$$k_{\text{corr}} = \frac{\Delta W}{At} \quad (2)$$

where t stands for the immersion period in minutes and A stands for the sample area in cm². All the experiments were conducted in stagnant aerated solutions. The standard deviation values among parallel triplicate experiments were found to be smaller than 5%, indicating good reproducibility. All the experiments were carried out in stagnant aerated solutions.

2.3 Electrochemical procedures

A common glass cell was assembled with three electrodes was used for the electrochemical processes. The electrodes comprised a working electrode made of Cu sheet welded with Cu wire for electrical connection and inserted into a Teflon tube and fixed with an adhesive, and the area exposed to the solution was ~1 cm²; a reference electrode made of SCE; and an auxiliary electrode made of Pt foil. The Cu electrode was immersed for 30 min in the solution prior to each electrochemical measurement so that the open circuit potential could reach a stable state.³⁴ To record and retain data, the electrochemical procedures were done utilizing a potentiostat/galvanostat ZRA analyzer (PCI4/750, Gamry Instruments, Warminster PA, USA) and the analysis of the data from tests was performed using E-Chem Analyst 5.5 software (Gamry E-Chem Analyst Version 5.5 software 7.8.5.8567). An ultra-circulating thermostat was used to conduct each experiment at 25 °C without deaerating the solutions. Each experiment was conducted with a fresh Cu electrode and electrolyte.

2.3.1 PDP measurements. The polarization test was performed by adjusting the potential ±250 mV *versus* OCP with a 0.2 mV s⁻¹ sweep rate. The corrosion current density (i_{corr}) and

corrosion potential (E_{corr}) were determined from Tafel plots without and with varying MOE doses. The following equation was used to get the % IE of MOE based on i_{corr} and the Cu surface coverage (θ):

$$\% \text{ IE} = \theta \times 100 = \left[1 - \frac{i_{\text{corr}}}{i_{\text{corr}}^0} \right] \times 100 \quad (3)$$

where, i_{corr}^0 and i_{corr} , respectively, reflect the corrosion current's density without and with varying MOE doses.

2.3.2 EIS measurements. The EIS test was accomplished with an alternating current amplitude of 10 mV in the frequency region of 10⁵–10⁻¹ Hz. The % IE was derived from θ obtained from the EIS measurements using eqn (4):

$$\% \text{ IE} = \theta \times 100 = \left[1 - \frac{R_{\text{ct}}^0}{R_{\text{ct}}} \right] \times 100 \quad (4)$$

where R_{ct}^0 and R_{ct} stand for, respectively, the resistance to charge transfer without and with varying Sumac extract doses.

2.4 Surface analysis

The Cu surface was analyzed using SEM, EDX, AFM, and FTIR before and after 3 h of immersion in a corrosive acidic environment without and with 300 ppm (highest dose) MOE. Scanning electron microscopy (SEM) and energy-dispersive X-ray analysis (EDX) were performed on a JEOL device (JSM IT-100, Japan). Atomic force microscopy (AFM) was also applied as it is an effective method for studying the surface morphology of Cu alloys at the nano or micro scale, and the data were analyzed using Nanosurf C3000 software, version 3.5.0.31. Fourier-transform infrared spectroscopy (FTIR) measurements were carried out using the total reflectance (ATR) mode and an iS 10 FTIR spectrometer from Thermo Fisher Scientific (USA).³⁵

3. Results and discussion

3.1 WL method

The effect of adding varying amounts (50–350 ppm) of MOE on Cu corrosion in a 1 M HNO₃ solution was evaluated using the WL method. The relationship between the impacts of various

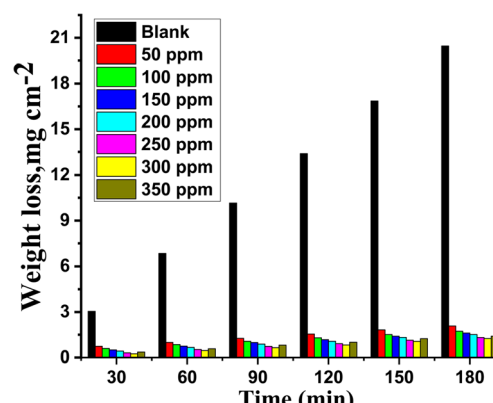


Fig. 1 WL versus time bar chart for the corrosion of Cu in 1 M HNO₃ in the presence and absence of varying doses of MOE at 25 °C.



doses of MOE on Cu given by the WL vs. time at 25 °C is depicted in Fig. 1. It was evident that the WL of Cu in the presence of the extract was significantly lower than that obtained in the blank solution. Additionally, Fig. 1 shows that the rate of Cu corrosion in nitric acid increased with the increase in contact time, but was reduced with the increase in MOE dosage, showing that the extract molecular layer adsorbed on the Cu surface caused a drop in WL. This layer protects the metal's corrosive sites and keeps the metal from corroding in the corrosive environment.^{36,37} This method has proven to be the most accurate method for determining the inhibition efficiency (% IE) and corrosion rate (k_{corr}). According to the data in Table 2, increasing the dose of MOE up to 300 ppm caused the corrosion rate to decrease and IE to increase. The addition of a concentration of 350 ppm led to a lower inhibition efficiency than at 300 ppm. Because of the physical adsorption process, the inhibition efficiency decreased to 92.5%, as indicated in Table 2. The solution became saturated and the inhibition efficiency decreased when the inhibitor concentration surpassed 300 ppm, which was this considered the optimum concentration. Additionally, there is a chance that the molecular extract in the solution and the extract affixed to the metal surface could interact strongly.^{38,39} The coating formed from the extract may be released into the solution as a result of this interaction. Since the amount calculated is directly proportional to the level of resolution, the WL test is typically chosen. In the solutions with and without extract, the linear fluctuation of WL over time showed that there were no insoluble surface layers caused by corrosion, whereby the inhibitor MOE was first adsorbed on the surface of the Cu alloy and subsequently reduced.

3.2 Temperature effect

Through the use of WL tests, the impact of different temperatures (25 °C, 30 °C, 35 °C, 40 °C, and 45 °C) on the corrosion of Cu in 1 M HNO₃ in the presence and absence of different doses of MOE extract was investigated. Table 3 displays the estimates of the CR and % IE derived from the WL tests for different doses of the extract in 1 M HNO₃ solution at different temperatures. The findings show that an increase in the extract dose led to a decrease in CR value and an increase in % IE. This is a result of the extract's increasing degree of adsorption and subsequent covering of the Cu surface as the extract dosage was increased.⁴⁰ The decrease in % IE with increasing the temperature shows that the extract may be adsorbed physically on the Cu surface.

Table 2 k_{corr} , θ , and % IE for the varying doses of MOE at 25 °C

Conc., ppm	k_{corr} mg cm ⁻² min ⁻¹	θ	% IE
Blank	0.11159	—	—
50	0.01286	0.885	88.5
100	0.01084	0.903	90.3
150	0.00982	0.912	91.2
200	0.0087	0.922	92.2
250	0.00757	0.932	93.2
300	0.00690	0.938	93.8
350	0.00837	0.925	92.5

Table 3 Results of the WL tests (k_{corr} , in mg cm⁻² min⁻¹, θ , and % IE) for Cu in the presence and absence of MOE after 120 min at 30–45 °C

Con., ppm	30 °C		35 °C		40 °C		45 °C	
	k_{corr}	% IE						
Blank	0.1473	—	0.2188	—	0.2848	—	0.3275	—
50	0.0202	86.4	0.0343	84.3	0.0527	81.5	0.0690	78.9
100	0.0188	87.3	0.0316	85.5	0.0473	83.4	0.0634	80.7
150	0.0171	88.4	0.0286	86.9	0.0436	84.7	0.0611	81.4
200	0.0154	89.6	0.0253	88.5	0.0410	85.6	0.0562	82.9
250	0.0140	90.5	0.0231	89.5	0.0367	87.1	0.0502	84.7
300	0.0119	91.9	0.0202	90.8	0.0308	89.2	0.0427	87.0

The estimation of E_a^* for the corrosion of Cu in uninhibited and inhibited acid corrosive media was computed by employing the Arrhenius equation:⁴¹

$$\log k_{\text{corr}} = -E_a^*/2.303RT + \log A \quad (5)$$

where A is the pre-exponential Arrhenius constant. Straight lines were achieved by drawing $\log k_{\text{corr}}$ versus $1/T$ without MOE and at different doses of MOE (Fig. 2) with a slope of $-E_a^*/2.303R$. The entropy (ΔS^*) and enthalpy (ΔH^*) of activation of Cu corrosion in a corrosive acidic environment without and with different doses of MOE were calculated using eqn (6):⁴²

$$k_{\text{corr}} = RT/Nh \exp^{(\Delta S^*/R)} \exp^{(-\Delta H^*/RT)} \quad (6)$$

where h represents Planck's constant. Plotting $\log k_{\text{corr}}/T$ vs. $1/T$ with and without an adjusted dose of MOE yielded straight lines (Fig. 3). Table 4 displays the highest values of E_a^* and ΔH^* when MOE was added, suggesting that the physical adsorption of MOE took place on the Cu surface. Positive values for ΔH^* indicate an endothermic adsorption of MOE molecules on the Cu. Large and negative values of ΔS^* in the uninhibited and inhibited system imply that the activation complex in the rate-determining steps represented an association rather than dissociation step, meaning that a decrease in disordering took place on going from the reactants to the activated complex.^{43,44}

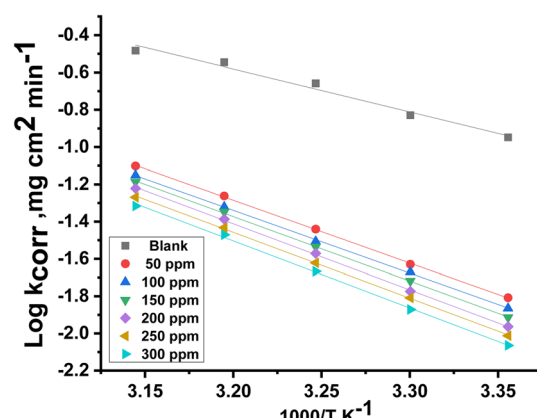


Fig. 2 Plot of $\log k_{\text{corr}}$ versus $1/T$ for Cu in the presence and absence of varying doses of MOE.



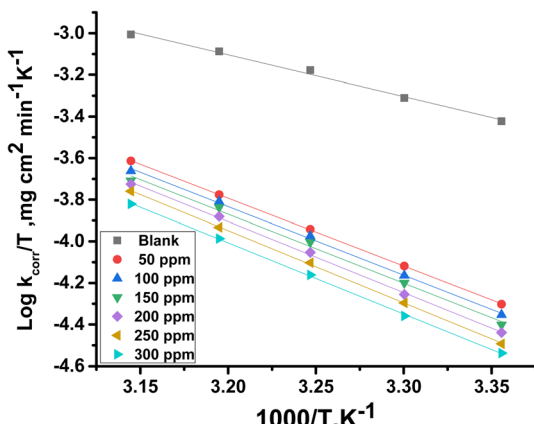


Fig. 3 Plot of $\log k_{\text{corr}}/T$ against $1/T$ for Cu in the presence and absence or varying doses of MOE.

Table 4 E_a^* , ΔH^* , and ΔS^* for Cu in the presence and absence of varying doses of MOE

C_{inh} , ppm	E_a^* kJ mol $^{-1}$	ΔH^* kJ mol $^{-1}$	$-\Delta S^*$ J mol $^{-1}$ K $^{-1}$
Blank	46.9	44.6	120
50	65.9	63.4	98
100	67.7	65.3	94
150	69.2	66.6	91
200	69.4	66.3	90
250	70.0	67.4	88
300	70.7	68.6	88

3.3 Adsorption consideration

To identify the corrosion mechanism, numerous adsorption isotherms have been used. Several adsorption isotherm equations, including the Langmuir, Freundlich, Temkin, and Frumkin, were solved using the experimental data derived using the WL approach. The isotherm that fitted the experimental data the best was selected using the correlation coefficient (R^2). The results were consistent with Langmuir's isotherm (Fig. 4) for adsorption (eqn (7)), which uses the subsequent equation to relate the metal surface coverage (θ) to the additive dose (C_{inh}):

$$\frac{C_{\text{inh}}}{\theta} = \frac{1}{K_{\text{ads}}} + C_{\text{inh}} \quad (7)$$

Within the given context, the dose of the inhibitor (measured in ppm) inside the bulk electrolyte is indicated as C , the surface coverage degree is θ , and the adsorption constant is K_{ads} . Plotting C/θ against C revealed that the slope of the Langmuir adsorption isotherm was close to unity and that the result showed the intercept was $1/K_{\text{ads}}$. The slope's deviation from unity can be explained by the reciprocal repulsion or attraction between the adsorbed molecules of the extract on the Cu surface.⁴⁵ By utilizing eqn (7), the values of (K_{ads}) were determined. The Langmuir adsorption isotherm was chosen as the best isotherm fitting the experimental data based on the high correlation coefficient ($R^2 > 0.9789$). The adsorption constant, K_{ads} , obtained from eqn (8) of the Langmuir adsorption

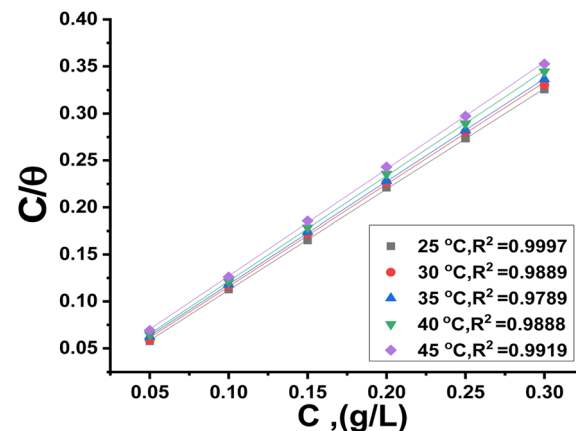


Fig. 4 Langmuir isotherm model for MOE for the liquefaction of Cu in 1 M HNO_3 .

isotherm, is specifically related to the free energy of adsorption, $\Delta G_{\text{ads}}^\circ$, by the relation:

$$\Delta G_{\text{ads}}^\circ = -RT\ln(55.5 \times K_{\text{ads}}) \quad (8)$$

where the numerical value 55.5 corresponds to the solution's water molarity, indicating the number of water particles per unit volume, measured in M^{-1} units. As is known, one crucial thermodynamic parameter for characterizing the adsorption process is $\Delta G_{\text{ads}}^\circ$. Table 5 lists the adsorption parameters for the obtained MOE. The achieved negative values of $\Delta G_{\text{ads}}^\circ$ decreased with increasing the temperature, indicating the greater stability of the adsorbed layer at low temperature, as shown by the data in the Table 5, indicating the spontaneous action of the MOE on the surface of the Cu. The $\Delta G_{\text{ads}}^\circ$ value was less than 20 kJ mol $^{-1}$, indicating physical adsorption, with values ranging from 20 to 40 kJ mol $^{-1}$ indicating mixed adsorption (physical and chemical). Similar to the results obtained,⁴⁶ the value of $\Delta G_{\text{ads}}^\circ$ in the current data was 23.1 kJ mol $^{-1}$, showing a mixed type inhibitor with physisorption being more relevant.

The enthalpy of adsorption ($\Delta H_{\text{ads}}^\circ$) was computed utilizing the following Vant Hoff equation:

$$\log K_{\text{ads}} = \frac{-\Delta H_{\text{ads}}^\circ}{2.303RT} + \text{constant} \quad (9)$$

Plotting $\log K_{\text{ads}}$ versus $1/T$ produced a straight line, as shown in Fig. 5. The adsorption entropy ($\Delta S_{\text{ads}}^\circ$) can be calculated as follows:

$$\Delta S_{\text{ads}}^\circ = \frac{\Delta H_{\text{ads}}^\circ - \Delta G_{\text{ads}}^\circ}{T} \quad (10)$$

Table 5 displays the computed $\Delta H_{\text{ads}}^\circ$ and $\Delta S_{\text{ads}}^\circ$ values. The exothermal adsorption of MOE on the Cu surface was indicated by the negative sign of $\Delta H_{\text{ads}}^\circ$. Adsorption can be chemical or physical in an exothermic procedure. The negative sign of $\Delta S_{\text{ads}}^\circ$ indicated reduced turbulence upon transition from the reactant to the adsorbed metal. This supports the potency and adsorption power of MOE.



Table 5 Langmuir parameters for the adsorption of MOE on the Cu surface at varied temperatures

Temp., K	$K_{\text{ads}} \text{ M}^{-1}$	$-\Delta G_{\text{ads}}^\circ \text{ kJ mol}^{-1}$	$-\Delta H_{\text{ads}}^\circ \text{ kJ mol}^{-1}$	$-\Delta S_{\text{ads}}^\circ \text{ J mol}^{-1}$
298	198.1	23.1	47.0	77.2
303	153.6	22.8		75.1
308	113.2	22.3		72.5
313	81.4	21.9		69.8
318	61.5	21.5		67.5

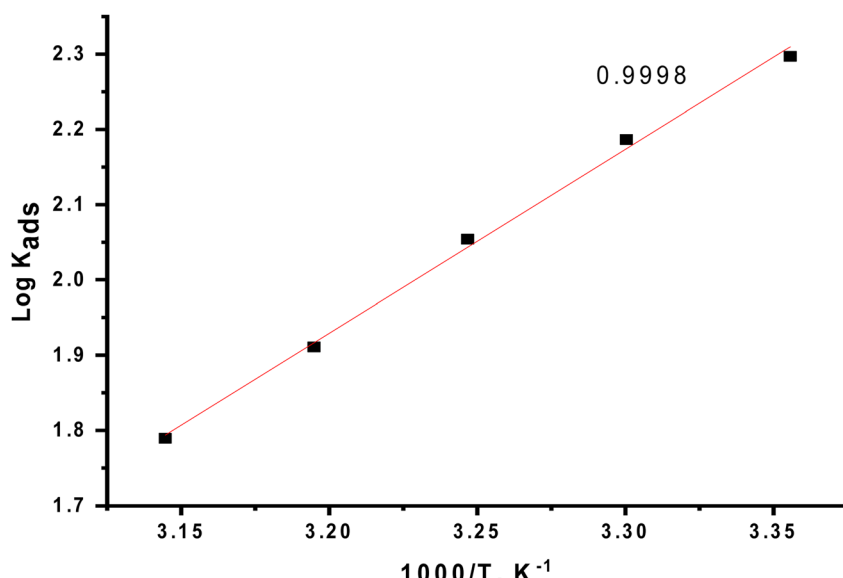


Fig. 5 Effect of varying the temperature on the free energies of the Langmuir isotherm.

3.4 PDP tests

PDP is an analytical technique that is essential to the study of corrosion inhibition because it yields important information regarding the tendency of a material toward passivation or pitting, as well as its rate of corrosion. By contrasting the polarization curves produced with and without inhibitors, it

also aids in estimating the efficacy of corrosion inhibitors. Polarization data were produced from the PDP measurement and utilized to examine the adsorption mechanism. Fig. 6 displays the PDP curves for Cu corrosion in 1 M HNO₃ with and without varying doses of MOE at 25 °C, showing that the anodic and cathodic plots moved to lower values, but largely on cathodic curves, indicating that the effect of the extract on the cathodic current was more pronounced than its effect on the anodic current. MOE can therefore, be regarded more as a cathodic-type inhibitor. According to the Stern–Geary theory,⁴⁷ a stronger corrosion resistance should also result from higher (β_a) and (β_c) values as depicted from Table 6, corresponding to lower i_{corr} values. According to Li *et al.*,⁴⁸ an inhibitor must have a minimum change in E_{corr} of ± 85 mV in order to be classified as either cathodic or anodic. The greatest displacement in this investigation was 28 mV, indicating that MOE was a mixed-type inhibitor. This finding implies that MOE was adsorbed by reaction at the Cu sites, which decreased the surface area available for the cathodic reactions and metal dissolution. The corrosion rate was computed using these parameters. The results of the electrochemical parameters at different MOE doses are listed in Table 6. The addition of 300 ppm produced the best inhibitory efficiency value of 91.1% (Table 6). This finding suggests that raising the dose to 300 ppm will effectively slow down the pace of Cu corrosion. The relationship between

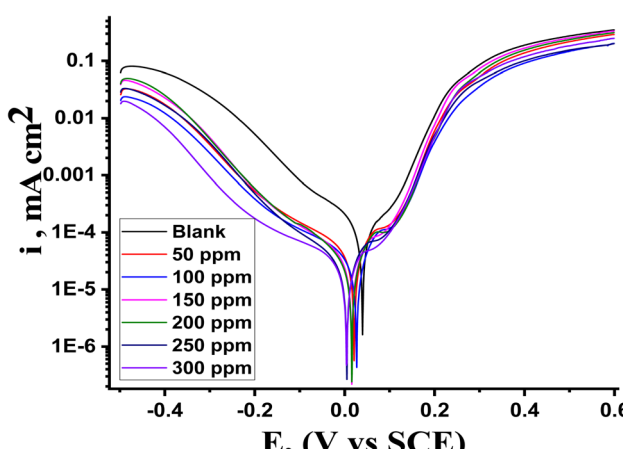


Fig. 6 Illustration of the PDP curves showing the dissolving behavior of Cu in the presence and absence of MOE extract at 25 °C.



Table 6 Calculations of the corrosion parameters for Cu in 1.0 M HNO₃ with varying inhibitor doses

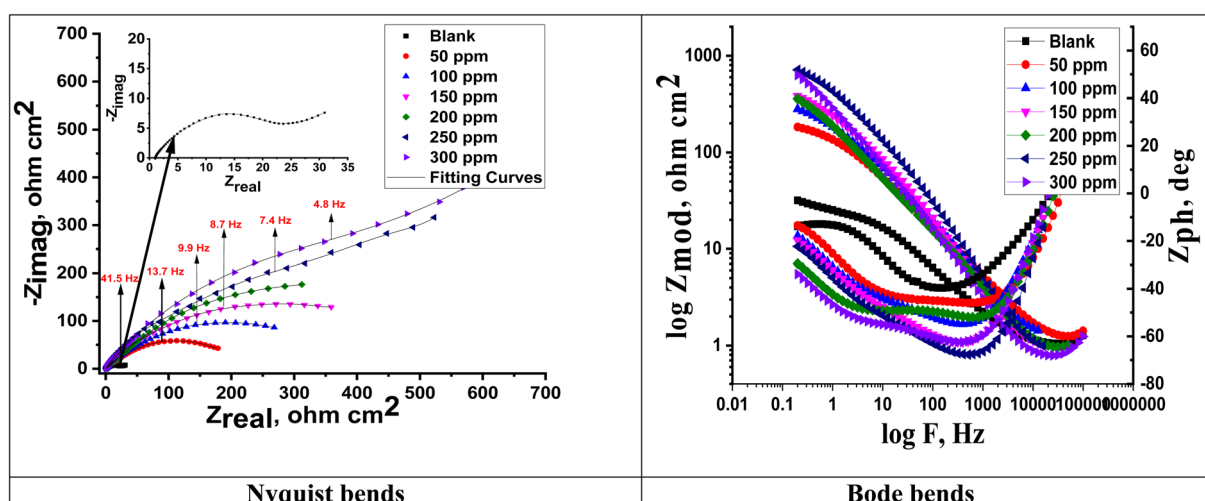
Conc. ppm	i_{corr} , $\mu\text{A cm}^{-2}$	E_{corr} , mV vs. SCE	β_a , mV dec ⁻¹	$-\beta_c$, mV dec ⁻¹	$k_{corr} \times 10^2$ mpy	θ	% IE
Blank	985	49	123	185	420	—	—
50	205	21	117	214	187	0.792	79.2
100	184	26	107	245	177	0.813	81.3
150	121	21	124	195	168	0.877	87.7
200	110	16	106	169	112	0.888	88.8
250	101	11	116	159	92	0.897	89.7
300	88	8	114	199	74	0.911	91.1

the rise in inhibition efficiency and the fall in current density was linear. The adsorption mechanism was examined using the PDP measurement findings. The anodic (β_a) and cathodic (β_c) Tafel slope values were essentially unchanged and parallel, demonstrating that the extract's addition had no effect on the mechanism. The i_{corr} values decreased as the extract dosages increased, suggesting that the percentage of IE rose as the extract dosage increased, demonstrating a respectable level of consistency with the results from alternative methods.

3.5 EIS test

Fig. 8 shows the electrochemical impedance (EIS) data that were examined using the suggested equivalent circuit diagram for Cu immersed in the test solution with and without different extract dosages. This figure shows the attained Nyquist and Bode curves for Cu dissolution in 1 M nitric acid with and without varying doses of MOE. A semicircle loop was used to identify the Nyquist diagrams, and proved that a charge-transfer process was followed for Cu metal disintegration.⁴⁹ Perfect semicircles were not produced by the Nyquist plot as predicted by the EIS theory. Both the surface inhomogeneities and the frequency dispersion are typically cited as the causes of the departure from the ideal semicircle.⁵⁰ Fig. 7 shows that the low-frequency area, where the impedance values grew in the presence of MOE compared to the lack of MOE, the radius of the circle rose as the dosage of MOE was increased, and therefore the charge-transfer

resistance to the corrosion reactions increased. Because of the adsorption of MOE at the Cu/solution contact,⁵¹ a high resistance was produced. The Bode graphs (Fig. 7) demonstrated how the phase angle shift continuously increased, which was clearly correlated with the increase in MOE adsorbed on the Cu surface. They also illustrate how the overall impedance increased with increasing MOE ($\log Z$ vs. $\log f$) and ($\log f$ vs. phase). Additionally, the Bode plots revealed a single peak component, suggesting that the one-time constant equivalent model with CPE provided the best fit for the EIS results. Furthermore, the Bode plots for the extract only showed one phase maximum associated with a single relaxation event, which was most likely caused by the charge-transfer process occurring at the metal/electrolyte interface. The matching circuits for the Cu and electrolyte are shown in Fig. 8a and b. Fig. 8a represent the equivalent circuit of the acid only and it consists of electrolyte resistance (R_u), charge-transfer resistance (R_{ct}), constant phase element (CPE), and W_d (the quadratic resistance, $W_d = 88.69 \times 10^{-3} \Omega \text{ cm}^2$). Fig. 8b represents the equivalent circuit for the corrosive solution containing MOE. It depicts a single charge-transfer reaction and is in good agreement with the outcomes of our experiments. To provide a more precise fit, the circuit incorporated a constant phase element (CPE) *in lieu* of a pure double-layer capacitor.⁵² CPE (Y_0 and n) was determined by the next equation to estimate the interfacial capacitance C_{dl} data:

Fig. 7 Nyquist and Bode curves for Cu liquefaction in 1 M HNO₃ in the presence and absence of varying doses of MOE at 25 °C.

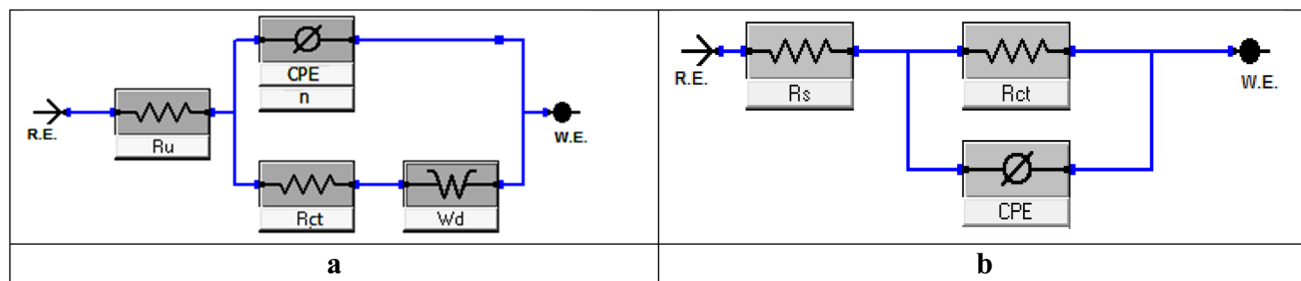


Fig. 8 Equivalent circuit to fit the EIS data for Cu displaying a Warburg impedance in 1 M HNO_3 (a). Equivalent circuit to fit the EIS data for Cu displaying one or more capacitive loops with MOE (b).

Table 7 Impedance parameters for Cu after immersion in 1.0 M HNO_3 in the presence of varying MOE doses at 25 °C

Conc., ppm	Y_0 , ($\mu\Omega^{-1} \text{s}^n \text{cm}^{-2}$)	n	R_{ct} , Ωcm^2	C_{dl} , $\mu\text{F cm}^{-2}$	W_d , Ωcm^2	θ	% IE	Goodness of fit, (χ^2)
Blank	518	0.961	29	436	88.69×10^{-3}	—	—	20.32×10^{-3}
50	319	0.973	186	295	—	0.641	64.1	22.47×10^{-3}
100	229	0.978	231	214	—	0.698	69.8	17.75×10^{-3}
150	187	0.987	279	179	—	0.801	80.1	20.14×10^{-3}
200	108	0.989	349	104	—	0.835	83.5	19.45×10^{-3}
250	101	0.991	522	98	—	0.856	85.6	14.7×10^{-3}
300	91	0.995	601	89	—	0.903	90.3	13.89×10^{-3}

$$C_{dl} = Y_0(\omega_{\max})^{n-1} \quad (11)$$

where Y_0 is the CPE magnitude, n is the variance CPE data (*i.e.*, $-1 \leq n \leq 1$), ω is the angular frequency ($\omega_{\max} = 2\pi f_{\max}$), and f_{\max} is the maximum frequency. The parameters obtained by fitted Nyquist arcs are summarized in Table 7. Aggressive species access to the metal surface was prevented by the

adsorption of the extract on the Cu surface, which blocked the active sites.⁵³ As the dosage rose, the homogeneity parameter n increased as well, showing a decrease in surface roughness and heterogeneity.⁵⁴ The impedance coefficients for Cu in 1 M nitric acid in the presence and absence of the varying doses of MOE were obtained. Table 7 shows there was a decrease in C_{dl} values and increase in R_{ct} values as the MOE dose increased, which

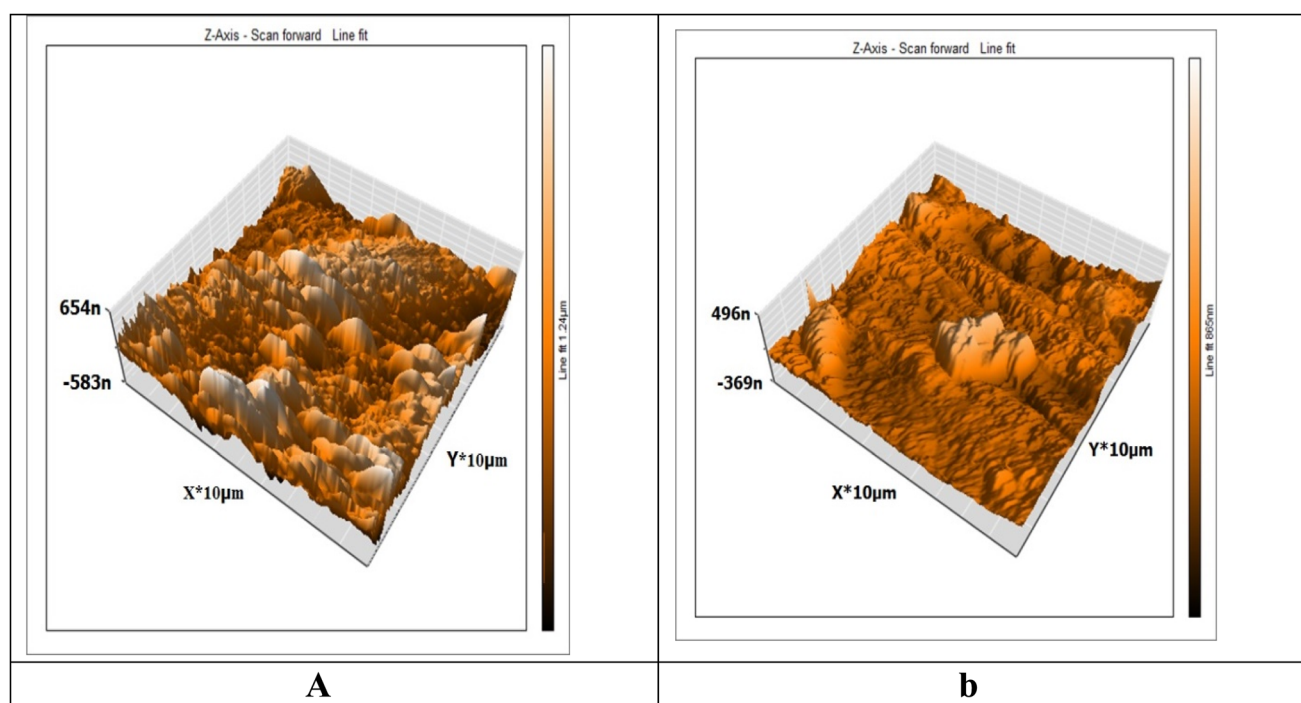


Fig. 9 3D AFM images for Cu specimen in 1 M HNO_3 only (a) and Cu specimen + 1 M HNO_3 + 300 ppm of MOE after 3 h immersion (b).



could be explained by the decrease in the local dielectric constant and/or an increase in the thickness of the electrical double layer.⁵⁵ This was due to the MOE molecules adsorbing on the Cu/interface with the solution and generating a protective coating on the Cu solution's interface.

3.6 Surface analysis

3.6.1 AFM studies. An effective method for examining the surface topography at the nano-to-micro scale is AFM. The inhibitor influence on the formation and advancement of corrosion at the metal or GLSS/solution contact has emerged as a novel research avenue.^{56,57} AFM is increasingly being used as a recognized technique to examine the roughness of metals, alloys, and glasses.⁵⁸ The surface morphology of the Cu was analyzed by AFM experiments after dipping in 1 M HNO₃ in the presence of 300 ppm MOE after 3 h immersion and was determined in terms of the surface roughness. The average values of the " S_a " roughness profile play a significant role in recognizing and reporting the effectiveness of a test inhibitor.⁵⁹ Among other things, roughness plays a role in explaining the nature of

the layer adsorbed on Cu. Fig. 9a shows the metal surface (white) was damaged by HNO₃, which had a high roughness value ($S_a = 277$), while Fig. 9b shows the Cu surface with the presence of 300 ppm MOE, which was not so corroded and had a lower roughness value ($S_a = 52$).

3.6.2 FTIR spectra. It is commonly known that the FTIR spectrophotometer is an effective instrument for determining the kind of bonding, namely the functional group(s), present in organic molecules. FTIR can be used to determine the type of chemical components adsorbed on the surface by analyzing surface variations. The interaction between the extract molecules and the metal surface was determined by FTIR analysis.⁶⁰ The FTIR spectra of an extract of MOE both before and after their adsorption on the Cu surface are shown in Fig. 10. The stretching vibration of the O-H stretch corresponded to the peak at 3343 cm⁻¹. This peak was modified to 3355 cm⁻¹ in the spectrum of the sample collected from the metal surface. It could be seen from Fig. 10 that there was a change in frequencies between the spectra of the MOE and the corrosion product after Cu was immersed, suggesting that the MOE

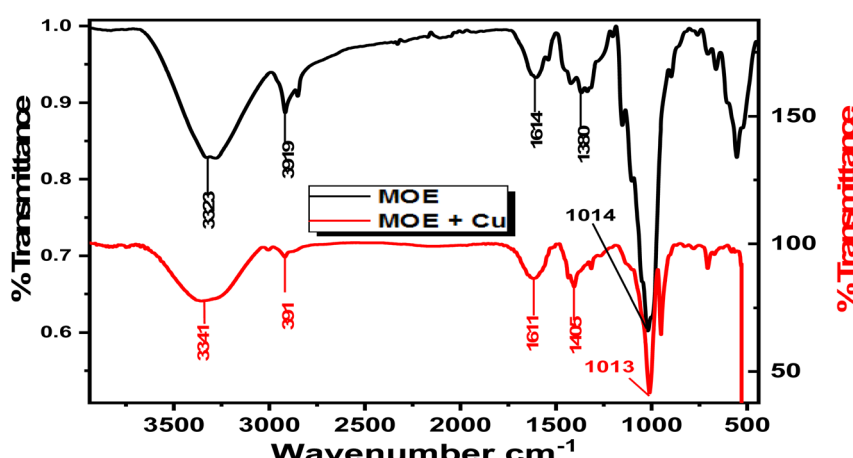


Fig. 10 FTIR spectra for free MOE (a) and the metal with MOE (b).

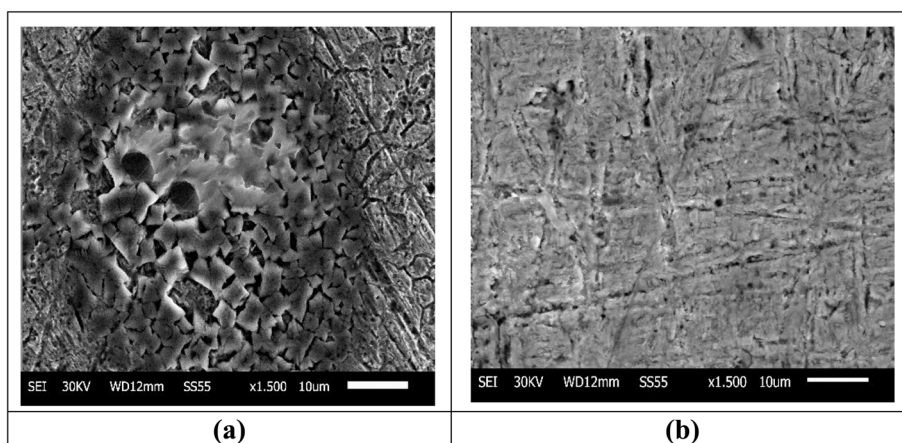


Fig. 11 SEM micrographs of Cu after one day of immersion in 1 M HNO₃ only (a), Cu after one day of immersion in 1 M HNO₃ with 300 ppm MOE (b).

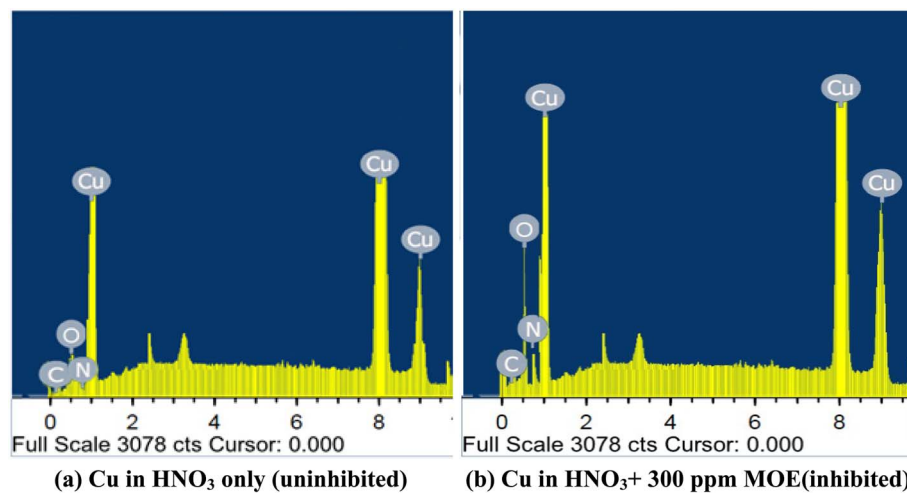


Fig. 12 EDX analysis of Cu after exposure to 1 M HNO_3 (a) and in the presence of MOE (300 ppm) after one day immersion.

interacted with the Cu surface through the functional groups of the extract.

3.6.3 SEM studies. The morphology of the Cu samples before corrosion was smooth with scratches due to use of the emery paper. When the samples were immersed in 1 M HNO_3 , it resulted in the complete degradation of the microstructure of the Cu surface, leading to the formation of significant cracks, as shown in (Fig. 11a).⁶¹ On the other hand, when MOE was added, the extract molecules yielded a notable reduction in Cu damage⁵⁰ and the surface became smooth, resulting in complete surface coverage,⁶² as demonstrated in Fig. 11b.

Table 8 Cu surface components (mass%) prior to and after exposure to 1 M HNO_3 for one day without and with the presence of MOE (300 ppm)

Mass percentages	O	C	Cu	N
Uninhibited Cu surface	18.18	5.79	58.21	6.18
Inhibited Cu surface	23.04	7.98	69.33	7.56

3.6.4 EDX spectroscopy. The quantitative dose of the primary components found on the Cu surface could be determined from the EDX spectra.⁶³ Fig. 12 displays the EDX spectra for the Cu surface after one day of immersion in 1 M HNO_3 without and with 300 ppm MOE. Table 8 lists the spectral elements' mass percentages. The spectrum of the Cu surface without MOE proved the existence of the elements O, C, and Cu. The inhibited surface's spectrum (Cu surface in HNO_3 solution with MOE) showed that there were more O and N atoms present, indicating that MOE had been adsorbed on the Cu surface, generating a layer that shielded the Cu from HNO_3 attack. The analysis results firmly back the usage of MOE in 1 M HNO_3 as a Cu corrosion inhibitor.

3.7 Mechanism of corrosion inhibition

The adsorption process is influenced by various factors, including the interaction between Cu and the solution, the electrochemical potential, the chemical composition, and the

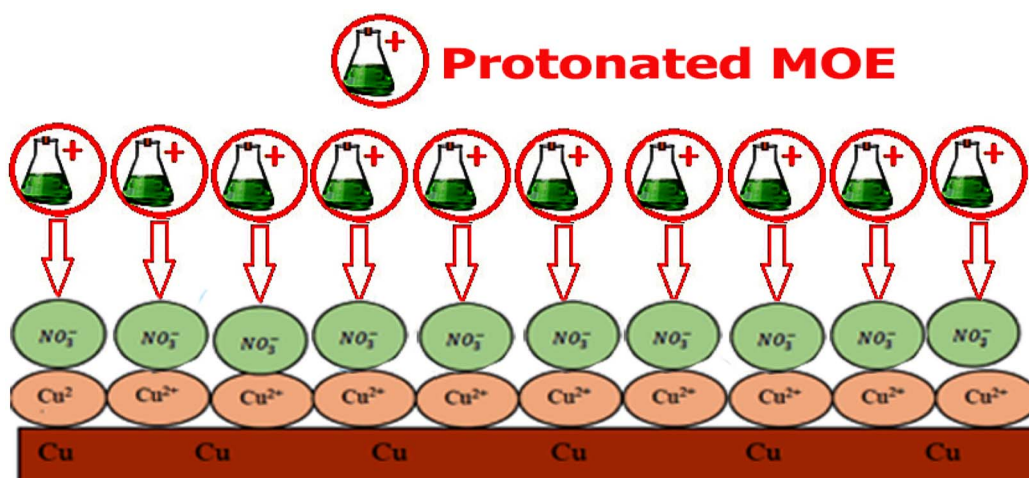


Fig. 13 Diagram showing the adsorption behavior of the extract.

surface properties of Cu. The adsorption phenomena are generally influenced by the charge on the metal surface, the kind of contact with the metal surface, and the chemical structure of the inhibitor. An adsorbent typically adheres to a surface by forming bonds or through chemical or physical adsorption. The extract adsorption on the Cu surface immersed in HNO_3 is a part of the inhibition mechanism. MOE may be found at the metal-solution contact from four different types of adsorption.⁶⁴ From the observations drawn from the various tests, corrosion hindrance of Cu in 1 M HNO_3 solutions by MOE, as noted from the WL, PDP, and EIS tests, was found to rely on the dosage and the nature of the extract. Some molecules of MOE may be protonated in the acid medium. So, it is difficult for these protonated molecules to adsorb on the positive Cu surface.^{65,66} Nitrate ions get adsorbed first on the Cu surface, and so the Cu surface becomes negatively charged, and then the protonated molecules of MOE get adsorbed on the nitrate layer, as shown below, forming a physisorption mechanism. Fig. 13 shows the adsorption behavior of the extract.

4. Conclusions

This work evaluated the inhibitory action of MOE for Cu in HNO_3 solution utilizing WL tests, and PDP and EIS techniques. The inhibition efficiency obtained from all the measurements showed fairly good agreement. The polarization experiments showed that the extract from MO functioned as a mixed-type inhibitor, delaying both cathodic and anodic processes without altering the corrosion mechanism. Impedance measurements demonstrated that the organic components of the MOE were adsorbed onto the corroding metal surface. It was discovered that the Langmuir adsorption isotherm was followed by the adsorption process from the acid. The values of the activation kinetic parameters derived from the experimental data supported the adsorption of MOE at various temperatures. The adsorbed protective film's AFM and FTIR morphology results on the surface of Cu verified MOE's high inhibitive effect.

Data availability

The data that support the findings of this study are available on request from the corresponding author.

Author contributions

Abd El-Aziz S. Fouda wrote the main manuscript text, Salah M. Rashwan supervision, Medhat M. Kamel and Mohamed Atef carried out the experimental part, Ahmed El-Hossiany, prepare the Tables and Figures. All the authors reviewed the manuscript.

Conflicts of interest

There are no conflicts to declare.

Acknowledgements

Open access funding provided by The Science, Technology & Innovation Funding Authority (STDF) in cooperation with The Egyptian Knowledge Bank (EKB). The authors are indebted to Mansoura University and Suez Canal Universities for all support and the facilities provided.

References

- 1 M. A. Khaled, M. A. Ismail, A. A. El-Hossiany and A. S. Fouda, *RSC Adv.*, 2021, **11**, 25314.
- 2 A. S. Fouda, E. Abdel-Latif, H. M. Helal and A. El-Hossiany, *Russ. J. Electrochem.*, 2021, **57**, 159–171.
- 3 A. S. Fouda, M. A. Abd El-Ghaffar, M. H. Sherif, A. T. El-Habab and A. El-Hossiany, *Prot. Met. Phys. Chem. Surf.*, 2020, **56**, 189–201.
- 4 A. M. El Defrawy, M. Abdallah and J. H. Al-Fahemi, *J. Mol. Liq.*, 2019, **288**, 110994.
- 5 A. S. Fouda, H. M. Abdel-Wahed, M. F. Atia and A. El-Hossiany, *Sci. Rep.*, 2023, **13**, 17593.
- 6 T. Zhou, J. Yuan, Z. Zhang, X. Xin and G. Xu, *Colloids Surf., A*, 2019, **575**, 57–65.
- 7 G. Ji, S. Anjum, S. Sundaram and R. Prakash, *Corros. Sci.*, 2015, **90**, 107–117.
- 8 M. Mehdiipour, B. Ramezanzadeh and S. Y. Arman, *J. Ind. Eng. Chem.*, 2015, **21**, 318–327.
- 9 R. Sathiyanathan, S. Maruthamuthu, M. Selvanayagam, S. Mohanan and N. Palaniswamy, *Indian J. Chem. Technol.*, 2005, **12**(3), 356–360.
- 10 R. A. Anaee, M. H. Alzuhairi and H. A. Abdulla, *Asian J. Eng. Technol.*, 2014, **2**, 235–243.
- 11 K. H. Hassan, A. A. Khadom and N. H. Kurshed, *S. Afr. J. Chem. Eng.*, 2016, **22**, 1–5.
- 12 O. O. Dominic and O. Monday, *J. Chem. Technol. Metall.*, 2016, **51**, 302–314.
- 13 R. T. Loto, *Results Phys.*, 2018, **8**, 172–179.
- 14 F. Bouhlal, N. Labjar, F. Abdoun, A. Mazkour, M. Serghini-Idrissi, M. El Mahi, A. Skalli and S. El Hajjaji, *Egypt. J. Pet.*, 2020, **29**, 45–52.
- 15 H. Lahbib, S. Ben Hassen, H. Gerengi, M. Rizvi and Y. Ben Amor, *J. Adhes. Sci. Technol.*, 2021, **35**, 691–722.
- 16 A. S. Fouda, M. A. Ismail, M. A. Khaled and A. A. El-Hossiany, *Sci. Rep.*, 2022, **12**, 1–19.
- 17 X. Zhang, W. Li, G. Yu, X. Zuo, W. Luo, J. Zhang, B. Tan, A. Fu and S. Zhang, *J. Mol. Liq.*, 2020, **318**, 114080.
- 18 B. A. Abd-El-Nabey, A. M. Abdel-Gaber, M. E. S. Ali, E. Khamis and S. El-Housseiny, *Int. J. Electrochem. Sci.*, 2013, **8**, 7124–7137.
- 19 M. Shabani-Nooshabadi, F. S. Hoseiny and Y. Jafari, *Anal. Bioanal. Electrochem.*, 2014, **6**, 341–354.
- 20 T. V Sangeetha and M. Fredimoses, *J. Chem.*, 2011, **8**, S1–S6.
- 21 A. M. Shah, A. A. Rahim, S. A. Hamid and S. Yahya, *Int. J. Electrochem. Sci.*, 2013, **8**, 2140–2153.
- 22 S. Gudić, E. E. Oguzie, A. Radonić, L. Vrsalović, I. Smoljko and M. Kliškić, *Maced. J. Chem. Chem. Eng.*, 2014, **33**, 13–25.



23 M. Shabani-Nooshabadi, F. S. Hoseiny and Y. Jafari, *Mater. Trans. A*, 2015, **46**, 293–299.

24 P. Deivanayagam, I. Malarvizhi, S. Selvaraj and P. Deeparani, *Int. J. Multidiscip. Res. Dev.*, 2015, **2**, 100–107.

25 B. A. Abd-El-Nabey, S. El-Housseiny, G. A. El-Naggar, E. A. Matter and G. Esmail, *Phys. Chem.*, 2015, **5**, 49–62.

26 C. Rahal, M. Masmoudi, R. Abdelhedi, R. Sabot, M. Jeannin, M. Bouaziz and P. Refait, *J. Electroanal. Chem.*, 2016, **769**, 53–61.

27 F. Wedian, M. A. Al-Qudah and G. M. Al-Mazaideh, *Int. J. Electrochem. Sci.*, 2017, **12**, 4664–4676.

28 L. Bazzi, L. Bammou, A. Chaouay, R. Salghi, S. Jodeh, B. Hammouti and A. Amin-Alamie, *Port. Electrochim. Acta*, 2017, **35**, 187–200.

29 A. S. Fouada, S. E. Badr, A. M. Ahmed and A. El-Hossiany, *Int. J. Corros. Scale Inhib.*, 2021, **10**, 1011–1029.

30 P. Refait, C. Rahal and M. Masmoudi, *J. Electroanal. Chem.*, 2020, **859**, 113834.

31 Y.-T. Liu, P.-H. Gong, F.-Q. Xiao, S. Shao, D.-Q. Zhao, M.-M. Yan and X.-W. Yang, *Molecules*, 2018, **23**, 271.

32 *Standard Practice for Laboratory Immersion Corrosion Testing of Metals*, G3172, ASTM, Philadelphia, PA, 1990, p. , p. 401.

33 V. Vorobyova and M. Skiba, *J. Bio-Tribos-Corros.*, 2021, **7**, 1–11.

34 E. Peñaloza, C. Holandino, C. Scherr, P. I. P. de Araujo, R. M. Borges, K. Urech, S. Baumgartner and R. Garrett, *Molecules*, 2020, **25**, 4006.

35 E. B. Agbaffa, E. O. Akintemi, E. A. Uduak and O. E. Oyeneyin, *Sci. Lett.*, 2021, **15**, 23–42.

36 A. S. Fouada, S. A. Abd El-Maksoud, A. El-Hossiany and A. Ibrahim, *Int. J. Electrochem. Sci.*, 2019, **14**, 2187–2207.

37 A. S. Fouada, S. E. H. Etaiw, A. M. Ibrahim and A. A. El-Hossiany, *RSC Adv.*, 2023, **13**, 35305–35320.

38 A. M. Fekry and M. A. Ameer, *Int. J. Hydrogen Energy*, 2011, **36**, 11207–11215.

39 A. S. Fouada, S. M. A. Motaal, A. S. Ahmed and H. B. Sallam, *Biointerface Res. Appl. Chem.*, 2021, **12**, 230–243.

40 N. Raghavendra, L. V. Hublikar, S. M. Patil, P. J. Ganiger and A. S. Bhinge, *Bull. Mater. Sci.*, 2019, **42**, 1–11.

41 A. S. Fouada, A. F. Molouk, M. F. Atia, A. El-Hossiany and M. S. Almahdy, *Sci. Rep.*, 2024, **14**, 16112.

42 A. S. Fouada, S. A. Abd El-Maksoud, A. A. M. Belal, A. El-Hossiany and A. Ibrahim, *Int. J. Electrochem. Sci.*, 2018, **13**, 9826–9846.

43 M. B. Ibrahim, Z. Sulaiman, B. Usman and M. A. Ibrahim, *World*, 2019, **4**, 45–51.

44 A. Fouada, M. A. Azeem, S. Mohamed and A. El-Desouky, *Int. J. Electrochem. Sci.*, 2019, **14**, 3932–3948.

45 A. M. Alsabagh, M. A. Migahed and H. S. Awad, *Corros. Sci.*, 2006, **48**, 813–828.

46 P. Singh, E. E. Ebenso, L. O. Olasunkanmi, I. B. Obot and M. A. Quraishi, *J. Phys. Chem. C*, 2016, **120**, 3408–3419.

47 G. Serdaroglu and S. Kaya, *Org. Corros. Inhib. Synth. Charact. Mech. Appl.*, 2021, pp. 59–73.

48 W. Li, Q. He, S. Zhang, C. Pei and B. Hou, *J. Appl. Electrochem.*, 2008, **38**, 289–295.

49 S. Zhang, L. Hou, H. Du, H. Wei, B. Liu and Y. Wei, *Corros. Sci.*, 2020, **167**, 108531.

50 A. S. Fouada, A. El-Mekabaty, I. E. I. Shaaban and A. El-Hossiany, *Prot. Met. Phys. Chem. Surf.*, 2021, **57**, 1060–1075.

51 M. Eissa, S. H. Etaiw, E. E. El-Waseef, A. El-Hossiany and A. S. Fouada, *Sci. Rep.*, 2024, **14**, 2413.

52 M. El Achouri, S. Kertit, H. M. Gouttaya, B. Nciri, Y. Bensouda, L. Perez, M. R. Infante and K. Elkacemi, *Prog. Org. Coat.*, 2001, **43**, 267–273.

53 A. S. Fouada, S. Rashwan, A. El-Hossiany and F. E. El-Morsy, *J. Chem., Biol. Phys. Sci.*, 2019, **9**, 1–24.

54 J. R. Macdonald, *Ann. Biomed. Eng.*, 1992, **20**, 289–305.

55 N. A. Odewunmi, S. A. Umoren and Z. M. Gasem, *J. Environ. Chem. Eng.*, 2015, **3**, 286–296.

56 K. P. V. Kumar, M. S. N. Pillai and G. R. Thusnavis, *J. Mater. Sci. Technol.*, 2011, **27**, 1143–1149.

57 H. A. Ali, A. A. El-Hossiany, A. S. Abousalem, M. A. Ismail, A. S. Fouada and E. A. Ghait, *BMC Chem.*, 2024, **18**, 182.

58 B. Wang, M. Du, J. Zhang and C. J. Gao, *Corros. Sci.*, 2011, **53**, 353–361.

59 A. K. Singh and M. A. Quraishi, *Corros. Sci.*, 2011, **53**, 1288–1297.

60 J. M. Bennett, M. M. Tehrani, J. Jahanmir, J. C. Podlesny and T. L. Balter, *Appl. Opt.*, 1995, **34**, 209–212.

61 M. M. Motawea, A. El-Hossiany and A. S. Fouada, *Int. J. Electrochem. Sci.*, 2019, **14**, 1372–1387.

62 A. S. Fouada, S. E. H. Etaiw, D. M. Abd El-Aziz, A. A. El-Hossiany and U. A. Elbaz, *BMC Chem.*, 2024, **18**, 21.

63 P. Mourya, S. Banerjee and M. M. Singh, *Corros. Sci.*, 2014, **85**, 352–363.

64 M. A. Deyab, *J. Power Sources*, 2016, **325**, 98–103.

65 N. Soltani, N. Tavakkoli, A. Attaran, B. Karimi and M. Khayatkashani, *Chem. Pap.*, 2020, **74**, 1799–1815.

66 M. A. Ali, A. M. Ouf, A. El-Hossiany and A. Fouada, *Biointerface Res. Appl. Chem.*, 2022, **12**, 5116–5130.

